Molecular engineering of logic gate types by module rearrangement in 'Pourbaix Sensors': the effect of excited-state electric fields†

Jake C. Spiteri,[a] Sergey A. Denisov,[b] Gediminas Jonusauskas,[c] Sylwia Klejna,[d] Konrad Szaciłowski,[d] Nathan D. McClenaghan[b] and David C. Magri*[a]

Two types of fluorescent logic gates are accessed from two different arrangements of the same modular components, one as an AND logic gate (**1**) and the other as a PASS 0 logic gate (**2**). The logic gates were designed with an 'electron-donor–spacer$_1$–fluorophore–spacer$_2$–receptor' format and demonstrated in 1 : 1 (v/v) methanol/water. The molecules consist of ferrocene as the electron donor, 4-aminonaphthalimide as the fluorophore and a tertiary alkylamine as the receptor. In the presence of high H^+ and Fe^{3+} levels, regioisomers **1a** and **1b** switch 'on' as AND logic gates with fluorescence enhancement ratios of 16-fold and 10-fold, respectively, while regioisomers **2a** and **2b** are functionally dormant, exhibiting no fluorescence switching. The PASS 0 logic of **2a** and **2b** results from the transfer of an electron from the excited state fluorophore to the ferrocenium unit under oxidising conditions as predicted by DFT calcu-lations. Time-resolved fluorescence spectroscopy provided lifetimes of 8.3 ns and 8.1 ns for **1a** and **1b**, respectively. The transient signal recovery rate of **1b** is ~10 ps while that of **2b** is considerably longer on the nanosecond timescale. The divergent logic attributes of **1** and **2** highlight the importance of field effects and opens up a new approach for regulating logic-based molecules.

Introduction

As an extension of the molecular engineering aspects of molecular-logic based computation, it is imperative to explore design flexibility.[1–3] The first two molecular logic gates demonstrated by de Silva combined two selective receptors, two alkyl spacers and an anthracene fluorophore.[4,5] These examples provided the well-established 'fluorophore–spacer$_1$–receptor$_1$–spacer$_2$–receptor$_2$'[4] and 'receptor$_1$-spacer$_1$–fluorophore–spacer$_2$–receptor$_2$'[5] formats. Both examples functioned as two-input AND logic gates. The latter design provided a greater fluorescence switching ratio as the distance for electron transfer between receptor$_2$ and the fluorophore was reduced. Subsequently, de Silva later demonstrated a different pair of analogous switches that functioned as AND logic gates given the same chemical inputs.[6] However, due to structure-specific effects the logic gates could be modulated to give rise to other logic behaviour from elementary one-input H^+-driven PASS 0 and H^+-driven YES to Ca^{2+}-enabled, H^+-driven *off–on–off* ternary logic.

Recently, there has been much interest in optical molecular devices responsive to acid–base and redox chemistry.[7] For example, Tian and Qu have demonstrated dual responsive 4-aminonaphthalimide-based molecular shuttles incorporating photoinduced electron transfer (PET) and internal charge transfer (ICT) mechanisms.[8] In another example, Mukhopadhyay has reported a series of tetrastable naphthalenediimides as colorimetric combinatorial logic gates from radical-anion and anion-induced ICT states.[9]

Herein we now report the pH and redox dependent steady-state and time-resolved fluorescence and transient absorption spectroscopy of two pairs of 4-aminonaphthalimide regioisomers.[10] The regioisomer pairs **1** and **2** were designed to function as 'Pourbaix sensors'.[11] Four supramolecular models **1a–b** and **2a–b** were synthesised with the same modular format according to an 'electron-donor–spacer$_1$–fluorophore–

[a]*Department of Chemistry, Faculty of Science, University of Malta, Msida, MSD 2080, Malta. E mail: david.magri@um.edu.mt; Tel: +356 2340 2276*
[b]*Institut des Sciences Moléculaires, CNRS UMR 5255, University of Bordeaux, 33405 Talence, France. E mail: nathan.mcclenaghan@u bordeaux.fr*
[c]*Laboratoire Ondes et Matière d'Aquitaine, CNRS UMR 5798, University of Bordeaux, 33405 Talence, France. E mail: gediminas.jonusauskas@u bordeaux.fr*
[d]*AGH University of Science and Technology, Academic Centre for Materials and Nanotechnology, Mickiewicza 30, 30 059 Kraków, Poland. E mail: szacilow@agh.edu.pl*

†Electronic supplementary information (ESI) available: Synthetic details, NMR, IR, HRMS, DFT frontier molecular orbital diagrams, UV visible absorption, fluo rescence decay curves and spectra. See DOI: 10.1039/c8ob00485d

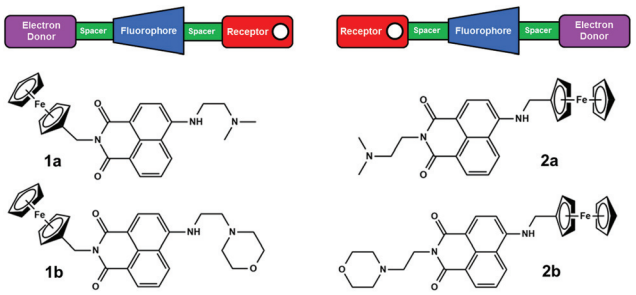

Fig. 1 The colour coded design concept of the two types of logic gates consisting of the same modular components arranged in two different ways and the molecular structures of series **1** and **2**.

spacer$_2$–receptor' arrangement (Fig. 1). Due to the asymmetric nature of the 4-aminonaphthalimide fluorophore, the regioisomer pairs **1** and **2** were synthesised by alteration of the imide and 4-amino substituents. Ferrocene was chosen as the oxidant-sensitive electron donor module and dimethylamine or morpholine as the proton receptor module. The receptor plays a dual role of being both an acceptor for protons and an electron donor for quenching the emissive excited state when unprotonated.[7] In the case of **1a** and **1b**, ferrocene is connected by a methylene spacer at the imide position and the dialkylamino moieties are connected to the 4-aminonaphthalimide position by an ethylene spacer. For **2a** and **2b** the ferrocene and dialkylamino modules are connected inversely (Fig. 1).

Based on molecular engineering first principles,[3] **1a–b** and **2a–b** were predicted to function the same as all module parameters are constant with the exception of the PET/ICT trajectories. During the course of the study we discovered that **1a–b** and **2a–b** exhibit remarkably different logic behaviour. This observation is an unprecedented example of functional discrimination by module rearrangement.[6] While many parameters controlling PET and ICT in supramolecular systems are generally well understood, our understanding of the influence of regiochemistry and electric field effects still remains underdeveloped.[10] This study provides new insight into the influence of field effects on PET/ICT phenomena and constitutes a new paradigm for controlling molecular logic gate functions.

Results and discussion

Logic gates **1a** and **1b** were synthesised from ferrocenylmethylamine[12] and 4-bromo-1,8-naphthalic anhydride in 2-methoxyethanol to yield *N*-ferrocenyl-4-bromo-1,8-naphthalimide in 64% yield, which was reacted with *N*,*N*-dimethylethylenediamine or 4-(2-aminoethyl)morpholine to give **1a** or **1b** in 70% and 13% yield after purification. Molecules **2a** and **2b** were synthesised by refluxing 4-bromo-1,8-naphthalic anhydride with *N*,*N*-dimethylethylenediamine or 4-(2-aminoethyl) morpholine, respectively, in 1,4-dioxane to give the intermediates in 70% and 46% yield, followed by aromatic nucleophilic substitution with ferrocenylmethylamine. Purification by column chromatography gave **2a** and **2b** in 34% and 22% yield, respectively. Synthetic details and analytical spectroscopic data including ^{1}H & ^{13}C NMR, IR and HRMS are provided in the Experimental and ESI (Fig. S1–S16†).

The thermodynamics for the photo-initiated charge transfer processes, to a first approximation, are expected to be identical for the regioisomers **1** and **2**. The driving forces for PET are −0.63 eV and 0.07 eV from the ferrocene and tertiary amine to the excited fluorophore, respectively.[13] With polyaromatic molecular logic gates, such as those based on anthracene with substitutents at the 9 and 10 positions, these simple calculations based on the Weller equation are a good guide for predicting the feasibility of electron transfer reactions and molecular logic gate performance.[5,6] However, the 4-aminonaphthalimide fluorophore is a push–pull π-electron system with a 4-amino group as donor and the naphthalimide (specifically the carbonyl end) as acceptor.[10] Consequently, a considerable large dipole moment (11 D) exists in the singlet excited state with a positive charge at the 4-amino end, and a negative charge build-up at the imide carbonyl end. Gao and Marcus' theoretical study predicted the imide nitrogen atom is a node in the frontier orbitals (*vide infra*).[14]

Evidence for ICT character can be observed from the UV-visible absorption spectra. In 1 : 1 (v/v) MeOH/H_2O and 10^{-9} M H^+ **1a** and **1b** exhibit a broad absorption band at 445 nm (Fig. S17 and S18†). Titration with up to 10^{-4} M H^+ causes a 14 nm hypsochromic shift due to protonation of the tertiary amine, which is attributed to a less stable Frank–Condon excited state. Superposition of the absorption spectra as a function of pH reveals an isosbestic point at 435 nm. In contrast, titration of **2a** and **2b** as a function of H^+ results in practically no observable change in the absorption spectra (Fig. S17 and S18†). Table 1 provides a summary of the photophysical data.

Table 1 Photophysical data for **1** and **2** in 1 : 1 (v/v) MeOH/H_2O[a,b]

	1a	**1b**	**2a**	**2b**
$\lambda_{Abs\ (pH\ 9)}$/nm (log ε)[c]	445(4.23)	445(4.00)	451(4.05)	443(3.89)
$\lambda_{Abs\ (pH\ 4)}$/nm (log ε)[c]	432(4.20)	430(4.01)	452(4.06)	447(3.91)
λ_{Isos}/nm	435	435	[d]	[d]
λ_{Flu}[e]/nm	530	530	550	550
$\Delta\lambda$[f]/nm	95	95	115	115
FE[g]	16	10	<1	<1
pβ_{H^+}[h,i]	7.4	5.6	8.2	6.0
p$\beta_{Fe^{3+}}$[h]	4.6	4.6		
pβ_{H^+}[h,j]	8.1	5.8	7.6	5.7
τ_f[k]/ns	8.3	8.1	[l]	[m]

[a] ~5 10 μM. [b] pH adjusted with aqueous NaOH and CH_3SO_3H solutions. [c] Molar absorptivity ε in L mol^{-1} cm^{-1}. [d] No isosbestic point observed. [e] Excited at λ_{Isos} at 10^{-4} M H^+ and 50 μM Fe^{3+}. [f] $\Delta\lambda$ λ_{Flu} λ_{Abs} at 10^{-4} M H^+ and 50 μM Fe^{3+}. [g] Fluorescence enhancement (FE) (I_{max} (50 μM Fe^{3+} at 10^{-4} M H^+)/(I_{max} (10^{-4} M H^+))). [h] Determined by log [(I_{max} I)/(I I_{min})] log[H^+] + log β_{H^+}. [i] In the absence of Fe^{3+}. [j] In the presence of 50 μM Fe^{3+}. [k] τ measured at 10^{-4} M H^+ with 50 μM Fe^{3+}. [l] Not measured. [m] Experimentally measured. Bi exponential.

The Boolean logic characteristics of regioisomers **1** and **2** in 1 : 1 (v/v) MeOH/H_2O are shown in Fig. 2. In the absence of threshold levels of H^+ or Fe^{3+} or both inputs, no fluorescence is observed for **1a** and **1b** (Fig. 1, top, vials A, B and C). As expected, addition of 10^{-4} M H^+ and 50 μM Fe^{3+} resulted in a bright green fluorescence visible to the naked eye (Fig. 1, vial D) in agreement with two-input AND logic. The emission spectrum exhibits a band centred at 530 nm. This band is a consequence of both the ICT state, resulting in a Stokes shift of 95 nm, and the prevention of PET, which allows for the fluorescent enhancement (Table 1, Fig. S17 and 18†). The fluorescence switching ratios between the 'off' and 'on' states are 16-fold and 10-fold for **1a** and **1b**. The fluorescence quantum yields (Φ_{Flu}) in the 'on' state are 0.041 and 0.032 for **1a** and **1b**, respectively.

The emission spectra of **2a** and **2b** exhibit a larger Stokes shift of 115 nm and a band centred at 550 nm. No fluorescence is observed with the naked eye in the absence of threshold levels of H^+ or Fe^{3+} or both inputs as anticipated. Rather unexpectedly, no fluorescence was observed in the presence of 10^{-4} M H^+ and 50 μM Fe^{3+} (Fig. 1, bottom, vials A, B, C and D). The combined outputs fit the definition of two-input PASS 0 logic (Table 2).

The reason for this divergent logic behaviour is intimately linked to the driving force for charge transfer, as mentioned earlier, which is sluggish from the tertiary amine to the 4-aminonaphthalimide fluorophore. Nonetheless, charge transfer from the dialkylamino receptor to the 4-aminonaphthalimide fluorophore readily occurs in **1a** and **1b** assisted by the positive electric field at the 4-amino end. In the case of **2a** and **2b**, charge transfer from the dialkylamino receptor is hindered by the negative electric field at the imide end.[14] Hence, the negative electric field at the imide end is a kinetic barrier for PET.

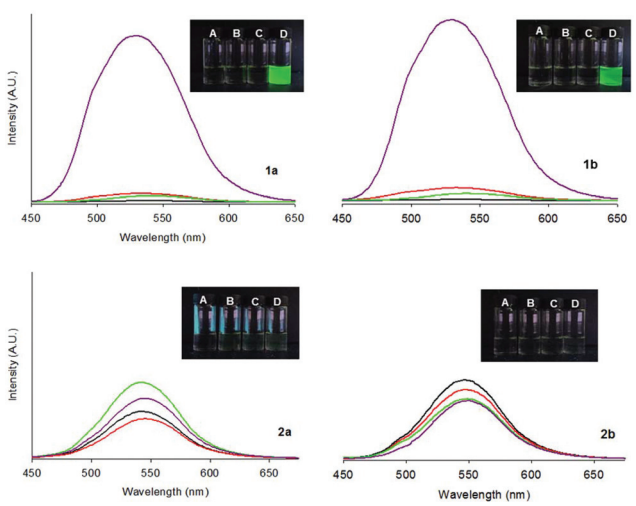

Fig. 2 Fluorescence spectra of 6 μM **1a**, 8 μM **1b**, 8 μM **2a** and 8 μM **2b** in 1 : 1 (v/v) methanol/water excited at 435 nm. Conditions for the vials irradiated with a 365 nm lamp and emission spectra are: (A) 10^{-9} M H^+, (B) 10^{-4} M H^+, (C) 10^{-9} M H^+, 50 μM Fe^{3+} and (D) 10^{-4} M H^+, 50 μM Fe^{3+}. The *y* axis scale on the plots of **2a** and **2b** are magnified. See Table 2 for relative fluorescence quantum yields.

Table 2 Truth tables for **1** and **2** and the fluorescence quantum yields (Φ_{Flu}) in parentheses in 1 : 1 (v/v) MeOH/H_2O[abcde]

Input$_1$ [f] (H^+)	Input$_2$ [g] (Fe^{3+})	**1a** AND	**1b** AND	**2a** PASS 0	**2b** PASS 0
0	0	0 (0.0004)	0 (0.0003)	0 (0.0010)	0 (0.0010)
1	0	0 (0.0025)	0 (0.0031)	0 (0.0006)	0 (0.0009)
0	1	0 (0.0014)	0 (0.0011)	0 (0.0020)	0 (0.0006)
1	1	1 (0.041)	1 (0.032)	0 (0.0014)	0 (0.0006)

[a] ~5 10 μM. [b] pH adjusted with aqueous NaOH and CH_3SO_3H solutions. [c] **1a** **1b** excited at λ_{isos} and **2a** **2b** at 435 nm. [d] Digital threshold limit set at $\Phi_{Flu} > 0.021$ for **1a** and $\Phi_{Flu} > 0.016$ for **1b**. [e] Estimated Φ_{Flu} errors for input (1,1) from an average of three experiments: **1a** (±0.005), **1b** (±0.005), **2a** (±0.003) and **2b** (±0.002). Relative Φ_{Flu} measured with reference to anthracene in ethanol (Φ_{Flu} 0.27). [f] High input level 10^{-4} M H^+. Low input level is 10^{-9} M H^+. [g] High input level 50 μM Fe^{3+}. Low input level no Fe^{3+} added.

However, we should note that unidirectional[10] and bidirectional[15] PET/ICT phenomena have been demonstrated with 4-aminonaphthalimide systems.

Another possible reason for the lack of fluorescence switching with **2a** and **2b** could be the formation of a weak intramolecular hydrogen bond on protonation.[10] Hydrogen bonding between the ammonium cation and one of the carbonyl oxygen atom may occur in the excited state *via* a six-membered transition state providing a non-radiative deactivation pathway. Similar phenomena have been observed with naphthalimide systems on complexation of metal ions such as Na^+ and Cu^+.[16,17]

Therefore, in order to gain further insight into the influence of the electric field effect on the excited state of **1** and **2** DFT calculations were performed. Energy level diagrams are shown in Fig. 3 and Fig. S19.† Frontier molecular orbitals of all four molecules are available in Fig. S20–S23.† The highest occupied molecular orbitals (HOMO) of **1a** and **1b** are localised on the ferrocene moiety, in both the neutral and amine-protonated forms. The lowest unoccupied molecular orbitals

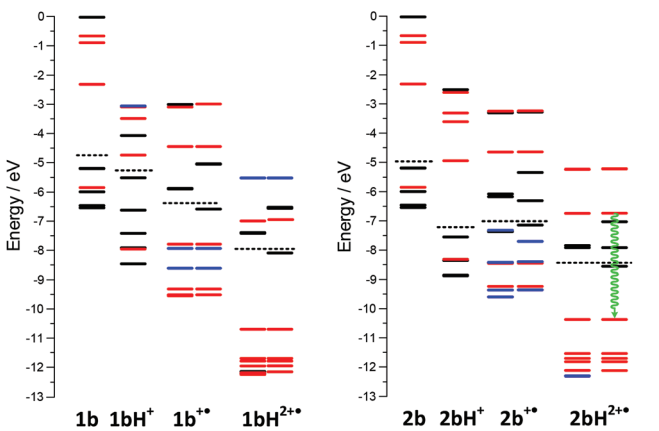

Fig. 3 Energy diagrams for neutral, protonated, oxidised, and protonated and oxidised forms of compounds **1b** and **2b**. Energy levels associated with ferrocene/ferrocenium, amine and 4 aminonaphthalimide are shown in black, blue and red, respectively. The green arrow highlights transitions from ferrocenium localised states.

(LUMO) reside exclusively on the 4-aminonaphthalimide in both the neutral and amine-protonated states. The methylene and ethylene spacers generally serve their purpose to effectively separate the fluorophore from the receptor and the electron donor. On oxidation, the HOMO orbital of **1a** involves the 4-aminonaphthalimide and amine moieties. For **1b** the HOMO is localised exclusively on the 4-aminonaphthalimide. In all cases, the LUMO resides on the ferrocenium moiety. The distinct change in the location of the HOMO and LUMO clearly illustrates ICT character. The incorporation of a methylene bridge in **2a** and **2b** results in a significant reduction in the HOMO delocalization.

Non-radiative deactivation of the 4-aminonaphthalimide fluorophore excited state is expected to be naturally feasible for the neutral, protonated and ferrocene-oxidised forms (*i.e.* **1a**, $\mathbf{1aH^+}$, $\mathbf{1a^{\bullet+}}$). Photoinduced electron transfer can occur from the ferrocene moiety (neutral and amine-protonated forms) and the amine moiety (neutral and oxidised forms). With $\mathbf{2aH^{2\bullet+}}$ and $\mathbf{2bH^{2\bullet+}}$ fluorescence quenching is also possible *via* non-radiative decay from the lowest 4-aminonaphthalimide-localised LUMOs to the 4-aminonaphthalimide HOMO *via* a series of ferrocenium-localised states (green arrow in Fig. 3, Fig. S19†). For $\mathbf{1aH^{2+}}$ and $\mathbf{1bH^{2+}}$ the ferrocenium-centred orbitals are localised at much higher energies and do not contribute to quenching of the luminescent state, in agreement with the experimental steady-state results.

We surmise that the reason no fluorescent enhancement is observed with regioisomers **2** is a consequence of an electric field effect. The ICT excited state dipole with its negative terminal at the imide end contributes to accelerate an electron transfer from the fluorophore to the ferrocenium unit across a positive electric field at the 4-amino terminus. Consequently, fluorescence is not observed under oxidising (and protonated) conditions in the case of **2a** and **2b**. With **1a** and **1b** electron transfer from the fluorophore to the ferrocenium unit is retarded by an attractive positive force situated at the 4-amino end and inhibited by a negative electric field at the imide nitrogen atom. Hence, regioisomers **1** experience a synergistic effect from the excited state electric field while regioisomers **2** experience an antagonistic effect.

The fluorescence lifetimes (τ_f) of **1a**, **1b** and **2b** were measured by time-resolved fluorescence spectroscopy in 1 : 1 (v/v) methanol/water under the four input conditions (Fig. S24–26†). The short-lived components of **1a** and **1b** correspond to the quenched PET/ICT lifetimes (<1.1 ns).[18] Upon protonation and oxidation the decay curves of **1a** and **1b** display single components (>99%) with fluorescence lifetimes of 8.3 ns and 8.1 ns, respectively. Hence, fluorescence becomes the predominant photophysical process.

The regioisomer **2b**, in stark contrast to **1b**, has bi-exponential components at all conditions including in the presence of high H^+ and Fe^{3+}. Time-resolved experiments confirm that fluorescence is not restored in the presence of both inputs in agreement with the steady-state fluorescence measurements. Once again, the long-lived and short-lived decay components correspond to back electron transfer and residual PET/ICT in the quenched state, respectively. Back electron transfer occurs on the nanosecond timescale of 4–6 ns, whereas the residual PET/ICT is <1 ns. The ICT character of the lowest energy transitions within the 4-aminonaphthalimide chromophore is much more pronounced in the case of **2a** and **2b** than in the case of **1a** and **1b**, which show mostly π–π^* character (Fig. S20–S23†). The spatial distribution of HOMOs and LUMOs in **1a** and **1b** overlap almost ideally, whereas in **2a** and **2b** the contours of HOMOs and LUMOs differ significantly.

Femtosecond transient absorption studies provide further insight into the regioisomer pair **1b** and **2b**.[11e,19] After excitation, **1b** undergoes a large charge density shift (<1 ps) within the 4-aminonaphthalimide fluorophore (Fig. 4). Ground state bleaching occurs at 450 nm (blue), stimulated emission at 550 nm (blue), and positive absorption at 460–500 nm and 650–700 nm due to redistribution of electron density (red) as a result of the ICT character.[10] The transient signal recovery rate proceeds on the order of ~10 ps. (Note: The negative perturbation at the zero delay is due to Kerr lensing produced by an intense femtosecond pump pulse with a weakly absorbing sample). In contrast, **2b** exhibits ground state bleaching at 380–440 nm (red) and stimulated emission between 500–620 nm (blue) (Fig. 5). The time delay is considerably

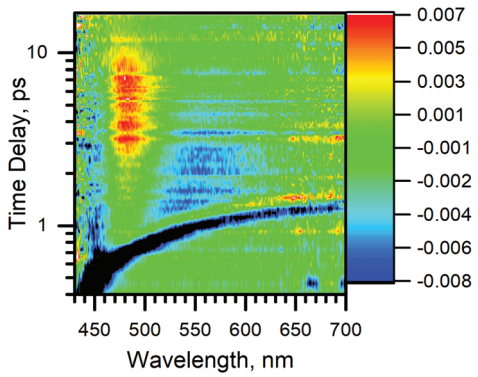

Fig. 4 Transient absorption map of **1b** in acetonitrile in the presence of 10^{-4} H^+ and 50 μM Fe^{3+}.

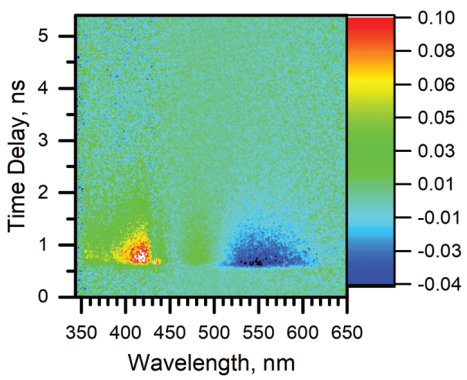

Fig. 5 Transient absorption map of **2b** in acetonitrile in the presence of 10^{-4} H^+ and 50 μM Fe^{3+}.

longer on the nanosecond timescale. This observation is consistent with the absence of fluorescence switching.

Conclusions

Two pairs of 4-aminonaphthalimide-based regioisomers **1** and **2** were synthesised with the intended purpose of simultaneous detection of pH and redox potential. Regioisomers **1** successfully operate as two-input AND logic gates for H^+ and Fe^{3+}, in agreement with the definition of 'Pourbaix sensors'.[7,11] In the absence of one or both inputs, the PET and/or ICT processes within **1a** and **1b** are efficient and shut off the fluorescence, while upon simultaneous protonation and oxidation, PET and ICT are non-competitive, resulting in a green fluorescence output. Regioisomers **2** are functionally dormant and behave as two-input PASS 0 logic gates. In other words, **2a** and **2b** do not behave as Pourbaix sensors because the negative charge at the imide and the positive charge at the 4-amino synergistically contribute to accelerate the transfer of an electron from the excited stated fluorophore to the ferrocenium unit under oxidising (and acidic) conditions.

The findings from this study open up a new approach for regulating the logic functions of fluorophores endowed with an ICT excited state and delineate the limitations of the 'electron-donor–spacer$_1$–fluorophore–spacer$_2$–receptor' format.

A future research direction is to rationally design a series of 4-aminonaphthalimide prototypes with varying intermediate driving forces for PET (-0.60 eV < ΔG_{PET} < 0.0 eV) with less strong electron donors compared to ferrocene at the 4-amino, and most notably at the imide positions, in order to evaluate the PET kinetics.[20] Application of Marcus' electron transfer theory would allow for determination of the activation barrier and electronic coupling factor.[21] Hence, a better understanding of this regulatory directional electron transfer phenomenon will undoubtedly contribute to the future development of various smart functional materials for application in the domains of photocatalysts,[22] artificial photosynthetic reaction centres,[23] multi-component molecular devices,[8] cellular imaging probes,[24] lab-on-a-molecule systems[25] and molecular steganography.[26]

Experimental

A list of chemicals and instrumentation are provided in the ESI.† Compounds **1a** and **1b** were synthesised from *N*-ferrocenyl-4-bromo-1,8-naphthalimide.[11d] Compounds **2a** and **2b** were synthesised from 4-bromo-1,8-naphthalic anhydride with the appropriate amine followed by substitution with ferrocenemethylamine. Full synthetic details and spectra are provided in the ESI.†

N-Ferrocenylmethyl-4-(2-dimethylaminoethyl amine)-1,8-naphthalimide (1a)

N-Ferrocenyl-4-bromo-1,8-naphthalimide (0.219 g, 0.462 mmol) and *N*,*N*-dimethylethylenediamine (5.0 mL, 46 mmol) were refluxed at 100 °C for 5 hours. The product was purified by column chromatography with silica gel and eluted with 4 : 1 (v/v) chloroform/methanol. Recrystallisation from 1 : 1 (v/v) acetone/water gave an orange solid in 70% yield. R_f = 0.73 (2 : 1 (v/v) CH_2Cl_2/MeOH); m.p. = 164–166 °C; ^{1}H NMR ($CDCl_3$, ppm): δ 8.55 (dd, 1H, J = 7.3, 0.9 Hz, Ar–*H*), 8.43 (d, 1H, J = 8.4 Hz, Ar–*H*), 8.10 (dd, 1H, J = 8.2, 0.9 Hz, Ar–*H*), 7.58 (dd, 1H, J = 7.8, 0.9 Hz, Ar–*H*), 6.63 (d, 1H, J = 8.5 Hz, Ar–*H*), 6.25 (m, 1H, –N*H*), 5.11 (s, 2H, –CH_2 spacer), 4.52 (t, 2H, J = 1.8 Hz, Cp), 4.20 (s, 5H, Cp), 4.06 (t, 2H, J = 1.8 Hz, Cp), 3.36 (m, 2H, –NHCH_2CH$_2$N), 2.72 (t, 2H, J = 5.8 Hz, –NHCH$_2$CH_2N), 2.33 (s, 6H, –N(CH_3)$_2$); ^{13}C NMR ($CDCl_3$, ppm): δ 164.5, 163.9, 149.6, 134.6, 131.1, 129.8, 126.4, 124.5, 123.1, 120.4, 110.1, 104.3, 83.8, 70.5, 68.6, 67.9, 56.9, 45.0, 40.1, 38.9; IR (KBr, cm^{-1}): 3393, 3092, 2955, 2866, 2828, 2783, 1684, 1636, 1582, 1541, 1385, 1369, 1339, 1300, 1246, 1188, 1126, 1105, 773; HRMS (ES-ToF): calculated $C_{27}H_{28}N_3O_2Fe$ [M + H]$^+$ 482.1531, found 482.1521.

N-Ferrocenylmethyl-4-(2-aminoethylmorpholine)-1,8-naphthalimide (1b)

N-Ferrocenyl-4-bromo-1,8-naphthalimide (0.759 g, 1.60 mmol) and 4-(2-aminoethyl)morpholino (0.50 mL, 11 mmol) were dissolved in 1,4-dioxane and refluxed for 4 hours at 95 °C. The product was purified by column chromatography with silica gel eluted with CH_2Cl_2 and 50 : 1 (v/v) CH_2Cl_2/MeOH. Recrystallisation from 1 : 1 (v/v) acetone/water gave an orange solid in 13% yield. R_f = 0.53 (20 : 1 (v/v) CH_2Cl_2/MeOH); m.p. = 218–224 °C (dec.); ^{1}H NMR ($CDCl_3$, ppm): δ 8.56 (dd, 1H, J = 7.3, 0.9 Hz, Ar–*H*), 8.43 (d, 1H, J = 8.4 Hz, Ar–*H*), 8.04 (dd, 1H, J = 8.5, 0.9 Hz, Ar–*H*), 7.60 (dd, 1H, J = 7.9, 0.9 Hz, Ar–*H*), 6.63 (d, 1H, J = 8.5 Hz, Ar–*H*), 6.21 (m, 1H, –N*H*), 5.11 (s, 2H, –CH_2 spacer), 4.52 (t, 2H, J = 1.8 Hz, Cp), 4.20 (s, 5H, Cp), 4.06 (t, 2H, J = 1.8 Hz, Cp), 3.78 (t, 4H, J = 4.5 Hz, –N(CH$_2$CH_2)$_2$O), 3.41 (m, 2H, –NHCH_2CH$_2$N), 2.82 (t, 2H, J = 5.9 Hz, –NHCH$_2$CH_2N), 2.57 (m, 4H, –N(CH_2CH$_2$)$_2$O); ^{13}C NMR ($CDCl_3$, ppm): δ 164.4, 163.8, 149.3, 134.4, 131.1, 129.6, 125.9, 124.7, 123.2, 120.3, 110.3, 104.4, 83.7, 70.5, 68.6, 67.9, 67.1, 56.0, 53.1, 38.9 (two peaks); IR (KBr, cm^{-1}): 3416, 3362, 3084, 2963, 2818, 1684, 1647, 1582, 1533, 1368, 1344, 1333, 1300, 1246, 1188, 1134, 1117, 1103, 775; HRMS (ES-ToF): calculated $C_{29}H_{30}N_3O_3Fe$ [M + H]$^+$ 524.1637, found 524.1639.

N,*N*-Dimethylethylenediamine-4-*N*-ferrocenyl methyl-1,8-naphthalimide (2a)

N,*N*-Dimethylethylenediamine-4-bromo-1,8-naphthalimide (0.440 g, 1.27 mmol) and ferrocenylmethylamine (0.301 g, 1.40 mmol) were dissolved in 10 mL of DMF and refluxed at 75 °C for 72 hours. The product was purified by column chromatography with silica gel eluted with gradient diethyl ether/methanol eluent (see ESI†). Removal of the solvent by rotary evaporator gave a reddish orange solid in 34% yield. R_f = 0.51 (3 : 1 (v/v) (CH$_3$CH$_2$)$_2$O/MeOH); m.p. = 165–170 °C (dec.); ^{1}H NMR ($CDCl_3$, ppm): δ 8.60 (dd, 1H, J = 7.4, 0.9 Hz, Ar–*H*), 8.50 (d, 1H, J = 8.4 Hz, Ar–*H*), 8.07 (dd, 1H, J = 8.5, 0.9 Hz, Ar–*H*), 7.64 (t, 1H, J = 7.9, 0.9 Hz, Ar–*H*), 6.80 (d, 1H, J = 8.4 Hz,

Ar–*H*), 5.46 (t, 1H, J = 4.5 Hz, –N*H*), 4.35 (t, 2H, J = 1.8 Hz, Cp), 4.33 (t, 2H, J = 7.2 Hz, –NCH_2CH$_2$N(CH$_3$)$_2$), 4.25–4.28 (m, 7H, Cp), 4.23 (d, 2H, J = 4.5 Hz, –HCH_2Cp), 2.66 (t, 2H, J = 7.2 Hz, –NCH$_2$CH_2N(CH$_3$)$_2$), 2.37 (s, 6H, –NCH$_2$CH$_2$N(CH_3)$_2$); ^{13}C NMR (CDCl$_3$, ppm): δ 164.7, 164.2, 148.8, 134.6, 131.2, 130.9, 125.7, 124.9, 123.2, 120.1, 110.6, 104.5, 84.2, 68.7, 68.6, 68.4, 57.1, 45.7, 43.1, 37.9; IR (KBr, cm^{-1}): 3441, 3084, 2944, 2860, 2820, 2773, 1734, 1684, 1653, 1648, 1636, 1577, 1541, 1506, 1456, 1362, 1339, 1242, 1124, 775; HRMS (ES-ToF): calculated $C_{27}H_{28}N_3O_2Fe$ [M + H]$^+$ 482.1531, found 482.1530.

4-(2-Aminoethyl)morpholine-4-*N*-ferrocenyl methyl-1,8-naphthalimide (2b)

4-(2-Aminoethyl)morpholine-4-bromo-1,8-naphthalimide (0.375 g, 0.960 mmol) and ferrocenylmethylamine (0.315 g, 1.47 mmol) were dissolved in 10 mL DMF and refluxed at 90 °C for 5 hours. The product was purified by column chromatography with silica gel with a gradient diethyl ether/methanol eluent (see ESI†). Removal of the solvent by rotary evaporator gave a reddish orange solid in 22% yield. R_f = 0.40 ((CH$_3$CH$_2$)$_2$O); m.p. = 94–98 °C; ^{1}H NMR (CDCl$_3$, ppm): δ 8.57 (dd, 1H, J = 7.3, 1.1 Hz, Ar–*H*), 8.47 (d, 1H, J = 8.2 Hz, Ar–*H*), 8.44 (dd, 1H, J = 8.5, 1.1 Hz, Ar–*H*), 7.66 (dd, 1H, J = 7.9, 1.1 Hz, Ar–*H*), 7.12 (d, 1H, J = 8.2 Hz, Ar–*H*), 5.70 (m, 1H, –N*H*), 4.33 (t, 2H, J = 7.1 Hz, –NCH_2CH$_2$N(CH$_2$CH$_2$)$_2$O), 4.20 (d, 2H, J = 5.6 Hz, –NHCH_2Cp), 4.19 (t, 2H, J = 1.8 Hz, Cp), 4.17 (s, 5H, Cp), 4.15 (t, 2H, J = 1.8 Hz, Cp), 3.69 (t, 4H, J = 4.6 Hz, –NCH$_2$CH$_2$N(CH$_2$CH_2)$_2$O), 2.70 (t, 2H, J = 7.1 Hz, –NCH$_2$CH_2N(CH$_2$CH$_2$)$_2$O), 2.59 (m, 4H, –NCH$_2$CH$_2$N(CH_2CH$_2$)$_2$O); ^{13}C NMR (CDCl$_3$, ppm): δ 164.6, 164.1, 160.1, 132.7, 131.2, 131.0, 125.3, 124.9, 123.1, 115.0, 113.4, 84.1, 68.6, 68.3, 68.2, 67.1, 56.2, 53.8, 44.8, 37.5; IR (KBr, cm^{-1}): 3320, 3080, 2953, 1684, 1657, 1655, 1589, 1456, 1423, 1390, 1381, 1346, 1242, 1142, 1113, 1009, 864, 779; HRMS (ES-ToF): calculated $C_{29}H_{30}N_3O_3Fe$ [M + H]$^+$ 524.1637, found 524.1633.

Computational

The ground and excited states electronic structure was computed with the TURBOMOLE suite of quantum chemical programs.[27] Hybrid DFT was employed within the B3-LYP exchange–correlation functional[28] and atom-centred triple-zeta valence basis functions, augmented by double polarization functions, TZVPP2.[29] Unrestricted Hartree–Fock method was used for open shell systems. Unconstrained optimization of the molecular geometry was carried out until the total energy was converged to 10^{-8} Ha in the self-consistent electronic loop. The minimum nature of the stationary point was confirmed by the vibrational analysis.

Conflicts of interest

There are no conflicts of interest to declare.

Acknowledgements

We thank the University of Malta for financial support. Prof. Robert M. Borg is acknowledged for NMR assistance and Maria Szaciłowska for assistance processing the DFT data. We extend our appreciation to the reviewers for their helpful comments. DFT calculations were performed at the Academic Computer Centre CYFRONET AGH within the computational grant "GRAPHENE" with funding from the European Union's Horizon 2020 research and innovation programme under grant agreement No 664786. The Embassy of France to Malta, the CNRS and the MCST (Malta Council for Science and Technology) are thanked for financial aid.

References

1 (*a*) A. P. de Silva, *Molecular Logic-based Computation*, The Royal Society of Chemistry, Cambridge, UK, 2013; (*b*) K. Szaciłowski, *Infochemistry. Information Processing at the Nanoscale*, Wiley, Chichester, UK, 2012; (*c*) *Molecular and Supramolecular Information Processing: From Molecular Switches to Logic Systems*, ed. E. Katz, Wiley, Weinheim, Germany, 2012.

2 (*a*) P. Remón and U. Pischel, *ChemPhysChem*, 2017, **18**, 1667; (*b*) O. Lustgarten, L. Motiei and D. Margulies, *ChemPhysChem*, 2017, **18**, 1678; (*c*) E. Katz, *ChemPhysChem*, 2017, **18**, 1688.

3 (*a*) A. P. de Silva, T. P. Vance, M. E. S. West and G. D. Wright, *Org. Biomol. Chem.*, 2008, **6**, 2468; (*b*) A. P. de Silva, T. S. Moody and G. D. Wright, *Analyst*, 2009, **134**, 2385; (*c*) A. P. de Silva, H. Q. N. Gunaratne, T. Gunnlaugsson, A. J. M. Huxley, C. P. McCoy, J. T. Rademacher and T. E. Rice, *Chem. Rev.*, 1997, **97**, 1515; (*d*) J. F. Callan, A. P. de Silva and D. C. Magri, *Tetrahedron*, 2005, **61**, 8551; (*e*) K. Szaciłowski, *Chem. Rev.*, 2008, **108**, 3481.

4 A. P. de Silva, H. Q. N. Gunaratne and C. P. McCoy, *Nature*, 1993, **364**, 42.

5 A. P. de Silva, H. Q. N. Gunaratne and C. P. McCoy, *J. Am. Chem. Soc.*, 1997, **119**, 7891.

6 J. F. Callan, A. P. de Silva and N. D. McClenaghan, *Chem. Commun.*, 2004, 2048. The fluorescence of a single-input H$^+$-driven PASS 1 logic gate is high irrespective of the H$^+$ level. Conversely, single-input H$^+$-driven PASS 0 shows no fluorescence whatever the H$^+$ level.

7 (*a*) D. C. Magri, A. D. Johnson and J. C. Spiteri, *J. Fluoresc.*, 2017, **27**, 551; (*b*) D. C. Magri, *Supramol. Chem.*, 2017, **20**, 741.

8 (*a*) H. Li, J.-N. Zhang, W. Zhou, H. Zhang, Q. Zhang, D.-H. Qu and H. Tian, *Org. Lett.*, 2013, **15**, 3070; (*b*) H. Zhang, J. Hu and D.-H. Qu, *Org. Lett.*, 2012, **14**, 2334; (*c*) H. Zhang, B. Zhou, H. Li, D.-H. Qu and H. Tian, *J. Org. Chem.*, 2013, **78**, 2091; (*d*) J.-N. Zhang, H. Li, W. Zhou, S.-L. Yu, D.-H. Qu and H. Tian, *Chem. – Eur. J.*, 2013, **19**, 17192.

9 M. R. Ajayakumar, G. Hundal and P. Mukhopadhyay, *Chem. Commun.*, 2013, **49**, 7684.

10 (*a*) A. P. de Silva, H. Q. N. Gunaratne, J. L. Habib-Jiwan, C. P. McCoy, T. E. Rice and J. P. Soumillion, *Angew. Chem., Ed. Int.*, 1995, **107**, 1728; (*b*) A. P. de Silva and T. E. Rice, *Chem. Commun.*, 1999, 163; (*c*) A. P. de Silva, A. Goligher, H. Q. N. Gunaratne and T. E. Rice, *ARKIVOC*, 2003, 229.

11 (*a*) T. J. Farrugia and D. C. Magri, *New J. Chem.*, 2013, **37**, 148; (*b*) D. C. Magri, *New J. Chem.*, 2009, **33**, 457; (*c*) D. C. Magri, M. Camilleri Fava and C. J. Mallia, *Chem. Commun.*, 2014, **50**, 1009; (*d*) J. C. Spiteri, J. S. Schembri and D. C. Magri, *New J. Chem.*, 2015, **39**, 3349; (*e*) A. D. Johnson, K. A. Paterson, J. C. Spiteri, S. A. Denisov, G. Jonusauskas, A. Tron, N. D. McClenaghan and D. C. Magri, *New J. Chem.*, 2016, **40**, 9917; (*f*) D. C. Magri and J. C. Spiteri, *Org. Biomol. Chem.*, 2017, **15**, 6706.

12 (*a*) P. D. Beer and D. K. Smith, *J. Chem. Soc., Dalton Trans.*, 1998, 417; (*b*) A. Baramee, A. Coppin, M. Mortuaire, L. Pelinski, S. Tomavo and J. Brocard, *Bioorg. Med. Chem.*, 2006, **14**, 1294.

13 A. Weller, *Pure Appl. Chem.*, 1968, **16**, 115. The driving forces for charge transfer are calculated as $\Delta G_{PET} = eF(E_{OX} - E_{RED} - E_S) - e^2/\varepsilon r$ where E_{OX} is the oxidation potential of ferrocene (0.45 V), tertiary amine (1.15 V) E_{RED} is the reduction potential of 4-aminonaphthalimide (−1.57 V), E_S is the excited state singlet energy of 4-aminonaphthalimide (2.55 V) and $e^2/\varepsilon r$ is the coulombic term (0.10 V). Potentials are versus SCE, e is the electric charge of an electron and F is the Faraday constant.

14 Y. Qin Gao and R. A. Marcus, *J. Phys. Chem. A*, 2002, **106**, 1956.

15 (*a*) E. B. Veale and T. Gunnlaugsson, *J. Org. Chem.*, 2008, **73**, 8073; (*b*) E. B. Veale, G. M. Tocci, F. M. Pfeffer, P. E. Kruger and T. Gunnlaugsson, *Org. Biomol. Chem.*, 2009, **7**, 3447.

16 (*a*) D. W. Cui, X. H. Qian, F. Y. Liu and R. Zhang, *Org. Lett.*, 2004, **6**, 2757; (*b*) Y. Xiao, M. Y. Fu, X. H. Qian and J. N. Cui, *Tetrahedron Lett.*, 2005, **46**, 6289.

17 H. Sharma, N. Kaur and N. Singh, *Inorg. Chim. Acta*, 2012, **391**, 83.

18 J. Gan, K. Chen, C. Chang and H. Tian, *Dyes Pigm.*, 2003, **57**, 21.

19 X. Li, N. Markandeya, G. Jonusauskas, N. D. McClenaghan, V. Maurizot, S. A. Denisov and I. Huc, *J. Am. Chem. Soc.*, 2016, **138**, 13568.

20 N. S. Hush, M. N. Paddon-Row, E. Cotsaris, H. Oevering, J. W. Verhoeven and M. Heppener, *Chem. Phys. Lett.*, 1985, **117**, 8.

21 R. A. Marcus and N. Sutin, *Biochim. Biophys. Acta*, 1985, **811**, 265.

22 (*a*) Q. Pan, F. Mecozzi, J. P. Korterik, D. Sharma, J. L. Herek, J. G. Vos, W. R. Browne and A. Huijser, *J. Phys. Chem. C*, 2014, **118**, 20799; (*b*) F. Franco, C. Cometto, C. Garino, C. Minero, F. Sordello, C. Nervi and R. Gobetto, *Eur. J. Inorg. Chem.*, 2015, 296; (*c*) J. Mech, K. Mech and K. Szaciłowski, *J. Mater. Chem. C*, 2015, **3**, 4148.

23 (*a*) M. R. Gunner, A. Nicholls and B. Honig, *J. Phys. Chem.*, 1996, **100**, 4277; (*b*) S. I. van Dijk, C. P. Groen, F. Hartl, A. M. Brouwer and J. W. Verhoeven, *J. Am. Chem. Soc.*, 1996, **118**, 8425.

24 (*a*) X.-F. Zhang, T. Zhang, S.-L. Shen, J.-Y. Miao and B.-X. Zhao, *J. Mater. Chem. B*, 2015, **3**, 3260; (*b*) Y. Yue, F. Huo, S. Lee, C. Yin and J. Yoon, *Analyst*, 2017, **142**, 30.

25 (*a*) K. Chen, Q. Shu and M. Schmittel, *Chem. Soc. Rev.*, 2015, **44**, 136; (*b*) B. Rout, L. Unger, G. Armony, M. A. Iron and D. Margulies, *Angew. Chem., Int. Ed.*, 2012, **51**, 12477; (*c*) D. C. Magri, G. J. Brown, G. D. McClean and A. P. de Silva, *J. Am. Chem. Soc.*, 2006, **128**, 4950.

26 T. Sarkar, K. Selvakumar, L. Motiei and D. Margulies, *Nat. Commun.*, 2015, **7**, 11734.

27 R. Ahlrichs, M. Bär, M. Häser, H. Horn and C. Kölmel, *Chem. Phys. Lett.*, 1989, **162**, 165.

28 (*a*) J. C. Slater, *Phys. Rev.*, 1951, **81**, 385; (*b*) A. D. Becke, *Phys. Rev. A*, 1988, **38**, 3098; (*c*) C. Lee;, W. Yang and R. G. Parr, *Phys. Rev. B: Condens. Matter Mater. Phys.*, 1988, **37**, 785; (*d*) A. D. Becke, *J. Chem. Phys.*, 1993, **98**, 5648.

29 A. Schafer, H. Horn and R. Ahlrichs, *J. Chem. Phys.*, 1992, **97**, 2571.